

Efficient Object Exploration and Object Presentation in TeleTA, Teleoperation System with Tactile Feedback

Dzmitry Tsetserukou and Susumu Tachi

University of Tokyo, Department of Information Physics and Computing, Japan

ABSTRACT

In order to achieve awareness of collision during teleoperation and to support operator with valuable information (object stiffness and shape), we elaborated approaches to object parameter identification and delivering this information to the operator's skin through tactile display. The tactile sensory ability of the remote manipulator allows collision detection and exploration of contacting object. A new type of tactile display that accounts for effectiveness of the information presentation, power consumption, ergonomics, and usability for particular teleoperation task was developed. The experimental results of object shape and stiffness presentation to the human's forearm revealed the most efficient vibration patterns.

KEYWORDS: Teleoperation, vibrotactile display, tactile feedback.

INDEX TERMS: H.5.2 [User Interfaces]: Haptic Interfaces; H.1.2 [User/Machine Systems]: Human Factors; I.3.6 [Methodology and Techniques]: Interaction techniques.

1 INTRODUCTION

The paper focuses on the teleoperation system **TeleTA** (**Tele**operation system with wearable **Tactile** display on the operator arm surface providing **Awareness** about slave robot collision) designed by us to achieve high level of maneuverability of robot arm in unstructured dynamic environment and to perform cooperative tasks with humans in a safe manner. We announce several distinctive contributions in this paper. New remote robot and sensory system for the operation in cluttered environment were developed. Distributed optical joint torque sensors and local admittance controllers endow our robot arm with the distinctive capability of safe interaction with surroundings along entire manipulator surface (including joints). The applied force vector can be calculated from the values of joint torques and contact point coordinates.

Master side (Fig. 1(a)) includes exoskeleton robot arm with 6 DOF (Fig. 1(b)) and tactile display BraTact to present cutaneous stimulation when collision with object is detected. The orientation of the human elbow is controlled by the tilt sensor. Teleoperated robot arm has 4-DOF: Roll, Pitch, Yaw joints of a shoulder, and Pitch joint of an elbow (Fig. 1(c)). Each joint is equipped with optical torque sensor directly connected to the output shaft of harmonic drive.

Proposed sensory system of slave robot (tactile skin to detect contact point and torque sensors distributed into each joint for measurement of applied force) patterns on the human tactile system. Our sense of touch can be separated into kinesthetic and coetaneous. Kinesthetic stimulations, produced by forces exerted

on body, are sensed by mechanoreceptors in the joints, tendons, and muscles enabling us to estimate forces being applied to body [1]. On the contrary, mechanoreceptors in the skin layers are responsible for cutaneous stimulation sensation that enables stimuli localization.

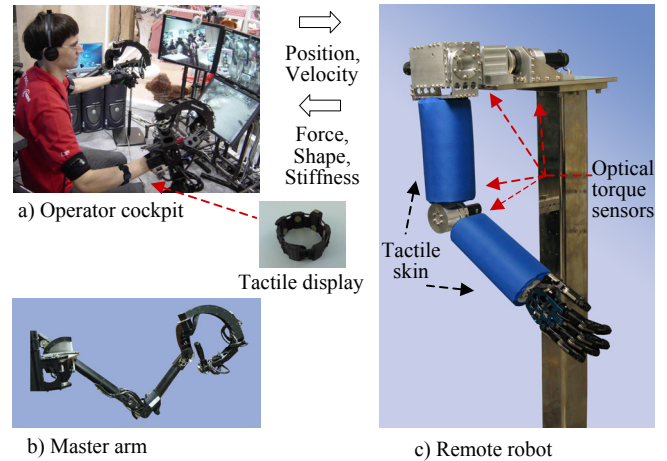


Figure 1. Robot teleoperation system TeleTA

The robot arm is covered with Kinotex tactile sensor measuring the pressure intensity through amount of backscattered light falling on photodetector [2]. The sensitivity, resolution, and dynamic range of this artificial skin are comparable to those of a human. It should be mentioned, however, that it is useful only for contact area and contact point recognition (cutaneous channel). Applied force sensitivity is very low due to large hysteresivity, high non-linearity of the output, and limited sensing range. The task of load measurement is accomplished by the developed optical torque sensors aimed at torque measurement in wide range with high accuracy (kinesthetic channel).

In order to recognize the contact region, we employed the watershed algorithm, an image processing segmentation technique that splits an image into areas based on the topology of the image [3]. The accurate estimation of the contact point can be obtained by computing the center of gravity of the contact pattern $c(x_c, y_c)$ of the neighborhood Ω by:

$$c(x_c, y_c) = \left(\frac{\sum_{x_i, y_i \in \Omega} x_i f_i(x_i, y_i)}{\sum_{x_i, y_i \in \Omega} f_i(x_i, y_i)}, \frac{\sum_{x_i, y_i \in \Omega} y_i f_i(x_i, y_i)}{\sum_{x_i, y_i \in \Omega} f_i(x_i, y_i)} \right), \quad (1)$$

where $f_i(x_i, y_i)$ is the pressure intensity level of the taxel i with coordinates (x_i, y_i) .

In the remainder of the paper we describe the methods of object parameter identification, techniques of object property presentation by the developed tactile display, and the results of user study on object property presentation.

7-3-1 Hongo, Bunkyo-ku, Tokyo.

E-mail: dima_teterukov@ipc.i.u-tokyo.ac.jp

2 OBJECT PARAMETER IDENTIFICATION WITH TACTILE SENSING

During the first stage of control the robot links rotate until one of them contacts the object. The control system detects the contact state using reference and actual torque values in the joints.

During contact transition we can acquire information about collision danger of contacting object through its stiffness estimation and represent this information to the operator. This can be done by establishing stiff contact through PD control of robot arm with high P-gain until joint torque exceeds the threshold value of 0.05 Nm. The robot was commanded to follow the trajectory in free space with constant angular velocity. An object was placed on this path so that the second link would contact it. The joint torque was recorded for the fourth joint while contacting with object. The Fig. 2(a-e) shows experimental results when link comes into contact with objects having different stiffness varying from very low rate to very high, namely, piece of sponge, rubber sponge, rubber, chemical wood, and aluminum, respectively. The time derivative of torque during impact is given in Fig. 2(f).

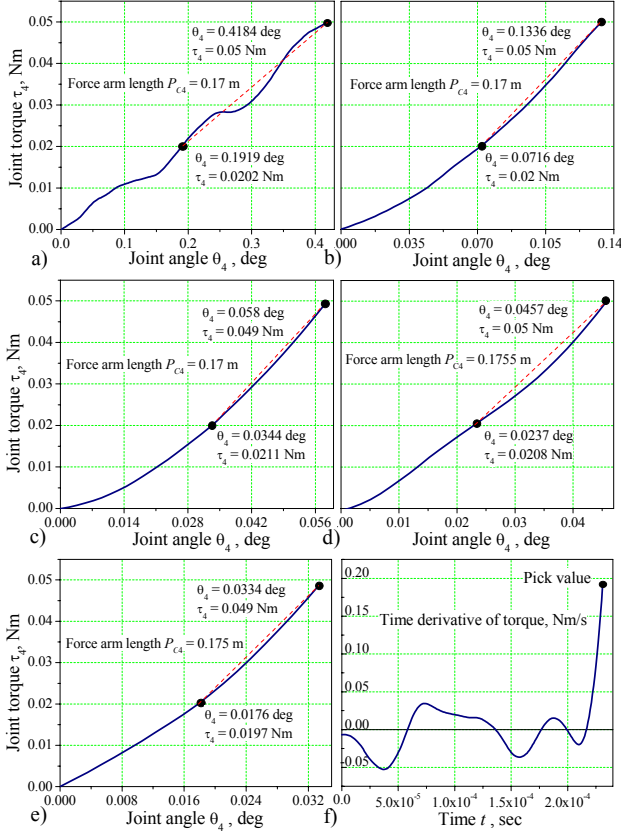


Figure 2. Experimental results of stiffness estimation

It is apparent from the plots presented above that the stiffer contacting object, the smaller angle of robot joint rotation. The elastic deformation of the object and inherent compliance of robot joints lead to rotation of robot arm by angle $\Delta\theta_i$ during contact transience (Fig. 3).

The distance, on which contact point C on the robot link surface 1 moves perpendicularly to the radius r_i under torque $\Delta\tau_i$, is equal to $r_i\Delta\theta_i$ (since the angle $\Delta\theta_i$ is fairly small). The unknown angle φ_i can be found by taking into account that $\angle CCB = \angle OCA = \varphi_i$:

$$\varphi_i = \arctan\left(\frac{OA}{CA}\right) = \arctan\left(\frac{h_i}{P_{Ci}}\right), \quad (2)$$

where h_i equals half of the robot link thickness.

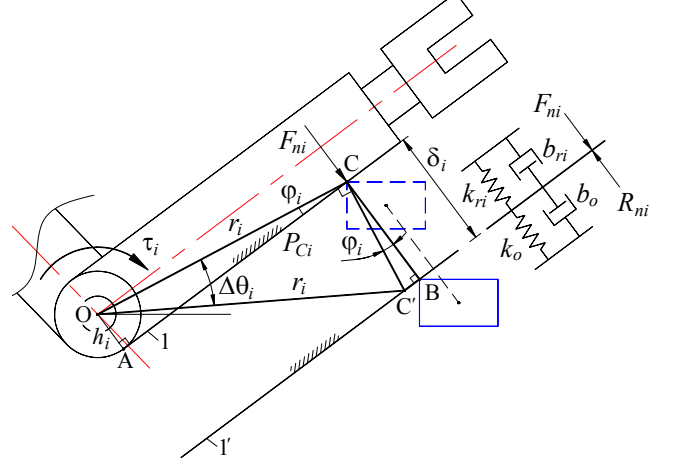


Figure 3. The scheme for elastic deformation calculation

The total elastic deformation is calculated from the right triangle ΔCBC as:

$$\delta_i = \Delta\theta_i r_i \cos(\varphi_i). \quad (3)$$

Radius of contact point trajectory r_i is found as $r_i = \sqrt{P_{Ci}^2 + h_i^2}$

through consideration of right triangle ΔCAO .

Now, we can easily solve for the total stiffness:

$$k_i = \frac{F_{ni}}{\delta_i} = \frac{\Delta\tau_i}{P_{Ci} \Delta\theta_i r_i \cos(\varphi_i)} = \frac{\Delta\tau_i}{P_{Ci} \Delta\theta_i \sqrt{P_{Ci}^2 + h_i^2} \cos(\arctan(h_i/P_{Ci}))}. \quad (4)$$

By linear approximation, we take into account only two values of θ_i for τ_i nearest to 0.02 Nm and 0.05 Nm. Then, from the experimental diagrams (Fig. 2(a-e)) we obtain $\Delta\theta_i$ and $\Delta\tau_i$ and list them in Table 1.

Table 1. Findings from experimental diagrams

Parameter	Sponge	Rubber sponge	Rubber	Wood
$\Delta\theta_i \cdot 10^{-4}$ [rad]	39.53	10.82	4.12	3.84
$\Delta\tau_i \cdot 10^{-2}$ [Nm]	2.98	3.0	2.79	2.92

The total elastic deformation δ_i is made up of elastic deformation caused by object compliance δ_o and one generated by joint flexibility δ_{ri} . That is, we can write:

$$\delta_i = \frac{F_{ni}}{k_i} = \delta_o + \delta_{ri} = \frac{R_{ni}}{k_o} + \frac{F_{ni}}{k_{ri}}, \quad (5)$$

where R_{ni} is the reaction, absolute value of which equals F_{ni} ; k_o and k_{ri} are stiffness of the object and stiffness of robot link, respectively.

The coefficient k_{ri} is mainly defined by torque sensor stiffness, harmonic drive stiffness, structural flexibility, and P-gain magnitude. Detailed examination has showed that complex

theoretical model of robot link stiffness can hardly provide accurate estimation of k_{ri} . Therefore, we can set the value of robot link stiffness close to total stiffness in the hardest contact case. This assumption is valid because during impact with hard environment, such as aluminum plate, the contact deformation of the object is too small to be accounted for ($k_o \approx \infty$). Thus, using Eq. (2)-(4) and the data presented in Fig. 2(a-e) we derive unknown value of k_{ri} :

$$k_{ri} = \frac{0.0293 \text{ Nm}}{0.175 \cdot 2.758 \cdot 10^{-4} \cdot 0.1776 \cdot 0.986 \text{ m}^2} = 3468.6 \frac{\text{N}}{\text{m}}$$

The object stiffness is calculated from the following equation:

$$k_o = \frac{k_{ri} \cdot k_i}{k_{ri} - k_i}, \quad (6)$$

where k_i is defined by Eq. (4).

Derived values of the total stiffness k_i and object stiffness k_o are given in Table 2.

Table 2. Total stiffness and object stiffness

Parameter	Sponge	Rubber sponge	Rubber	Wood
k_i [N/m]	260.8	959.3	2343.8	2469.0
k_o [N/m]	282.0	1325.9	7223.9	8562.9

The obtained results demonstrate strong correspondence of correlation among calculated object stiffness with that of real objects. Specifically, we can define that sponge and rubber sponge material are safe for interaction, but rubber, wood, and metal pose threat while striking the robot arm.

3 SHAPE RECOGNITION

Studies on human tactile perception show that edge or contour following is one of the common exploratory procedures that people use for the determination of object geometry [4]. We propose the tactile object shape recognition method based on the acquisition and formulation of information as image primitives. Tactile images are generated when robot arm registers a series of contact points with an object. Graphical modeling of the movement of the robot arm following along round contour is shown in Fig. 4.

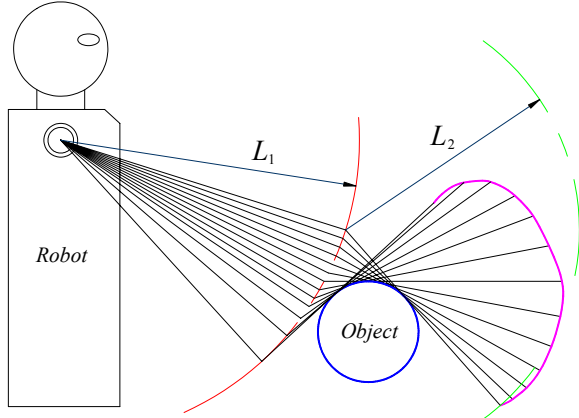


Figure 4. Circular shape following

The node points obtained by employing the contact point detection algorithm can be interpolated by B -splines. The spline method solving the connection problem that exists with other techniques, features superior controllability, and desired continuity [5]. B -spline curve is expressed as a convex combination of polygon vertex position vectors. To obtain C^2 continuity, we employ cubic uniform B -spline. The segment i of spline curve $P_i(t)$ is a cubic parametric polynomial described by:

$$P_i(t) = \frac{1}{6} \begin{bmatrix} t^3 & t^2 & t & 1 \end{bmatrix} \begin{bmatrix} -1 & 3 & -3 & 1 \\ 3 & -6 & 3 & 0 \\ -3 & 0 & 3 & 0 \\ 1 & 4 & 1 & 0 \end{bmatrix} \begin{bmatrix} P_{i-1} \\ P_i \\ P_{i+1} \\ P_{i+2} \end{bmatrix}, \quad (7)$$

where P_{i-1} , P_i , P_{i+1} , and P_{i+2} are the control points (preliminary calculated contact points); $i = 1, 2, \dots, n-2$; $n+1$ is the number of given control points; $t \in [0, 1]$ is the global parameter.

An actual spline curve is made of these curve segments $P_i(t)$. Let us estimate the error of object shape approximation by using proposed approach. We assume that object has circular contour of radius R , and the contact points P_{Ci} placed on it are equidistant (Fig. 5).

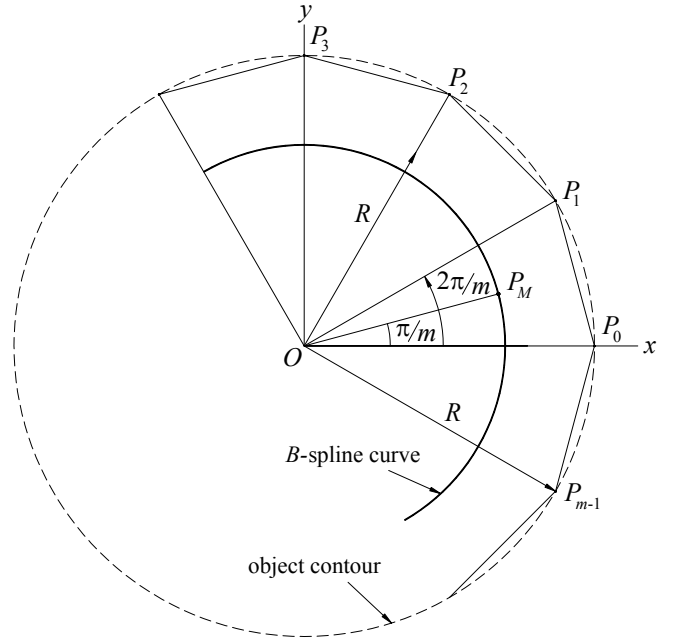


Figure 5. Method of object shape approximation

The coordinates of contact points P_{Ci} are defined by:

$$P_{Ci} = (R \cos \theta_i, R \sin \theta_i) = \left(R \cos \left(\frac{2\pi i}{m} \right), R \sin \left(\frac{2\pi i}{m} \right) \right), \quad (8)$$

where m is the number of control points (equals $n+1$), $i = 0, 1, \dots, m-1$. For the sake of simplification of further computations, we assume the radius R of one unit.

The worst approximation is obtained midway between control points, i.e. $P_i(0.5)$. The midpoint of a cubic segment, however, is easily derived from Eq. (7) as:

$$P_M = P_i(0.5) = \frac{1}{48} (P_{m-1} + 23P_0 + 23P_1 + P_2). \quad (9)$$

After substitution of the control point coordinates from Eq. (8) to Eq. (9) we have:

$$P_M = \left(\frac{(1 + \cos \theta)(11 + \cos \theta)}{24}, \frac{\sin \theta(11 + \cos \theta)}{24} \right), \quad (10)$$

where $\theta = 2\pi/m$.

The deviation E (%) from a true circle is expressed as:

$$E = \left(1 - \sqrt{P_M^2} \right) \times 100 = \frac{12 - (11 + \cos(2\pi/m)) \cos(\pi/m)}{12} \times 100.$$

The findings of deviation for different number of control points are listed in Table 3.

Table 3. Deviation from a true circle

m	12	16	20	24	28	32	36
E [%]	4.49	2.54	1.63	1.14	0.836	0.64	0.51

The proposed approach based on B -spline can therefore provide an excellent approximation to a circle. Since the robot angular iterations are sufficiently small, the number of control points is huge. This fact results in a very precise contour recognition.

The curvature of the curve segment i is calculated as:

$$P_i = \frac{P'_{ix}P''_{iy} - P'_{iy}P''_{ix}}{(P'^2_{ix} + P'^2_{iy})^{3/2}}. \quad (11)$$

The algorithm of contour recognition of the rectangular-shaped object is as follows. In presence of vertex, the lines intersect in one point. When coordinates of intersection point change drastically, the subsequent vertex is recognized. The line connecting two vertices defines the edge of the object.

More complicated shapes can be detected by combination of B -spline interpolation, vertex, and edges recognition. If the curve defining vectors P_{i-1} , P_i , P_{i+1} , and P_{i+2} lie collinear, the curve segment defined by those four position vectors degenerates to a line segment. This line segment connects continuously to the neighboring curve segments with continuity up to curvature vector. This feature is extremely useful in the case of complex shape recognition.

4 DEVELOPMENT OF THE ERGONOMIC TACTILE DISPLAY BRAFACT

In order to deliver the sense of object touch to the operator, the force-feedback devices [6], [7] (generating kinesthetic stimuli) and tactile-feedback system [8] (evoking cutaneous stimuli on local area of the skin) are widely applied. The devices of former type are able to exert strong forces on human body and limit user motion in a natural manner. However, they are cumbersome, have narrow workspace, and enable to generate force only at the human hand. When it comes to the contact presentation on the human arm, tactile displays are preferable ones. They can convey contact cues [9], direction [10], and distance [11] information. Recently, haptic gadgets displaying information on a large area of the human body are gaining increased attention by researchers. In [12], reconfigurable, wearable system TactaVest for delivering vibro-tactile stimuli is presented.

It can be seen from the papers presented above that, typically, the huge amount of actuators are arranged in regular grid pattern. It should be mentioned here, that heavy tactile display placed on the arm surface degrades the mobility and increases joint muscle loading. Therefore, our objective was to find out the approach to effective presentation of tactile information.

Several attempts were made to explore the human tactile patterns for effective communication with mobile devices [13], [14]. Chen *et al.* [15] examined the human ability to localize a single vibration source on dorsal and volar sides of the forearm near wrist. For the experiments a 3-by-3 tactor array was placed on the dorsal and volar parts of the wrist, respectively. An important finding was that on average only 4 tactor locations could be correctly identified on both sides of the wrist.

The developed tactile bracelet **BraTact (Bracelet with Tactors)** incorporates six vibration motors with holders linked by elastic band. Proposed shape takes advantage of the facts that we already used to wear bracelet-shaped watches and accessories, and that such shape of the tactile display can fit to the humans of different sizes. To enhance the localization ability, we arrange the tactors in a zigzag pattern (Fig. 6).

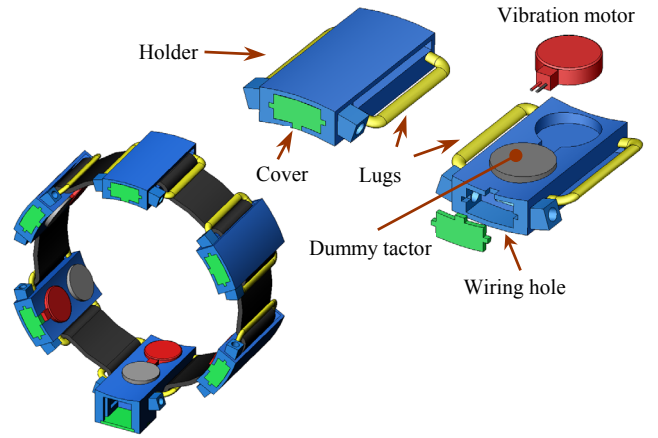


Figure 6. Tactile display BraTact

The inner surface of the holder has concave profile to match the curvature of human arm surface. The designed tactile bracelet is shown in Fig. 7.



Figure 7. Tactile bracelet

The small flat coreless vibration motors FM34F with diameter of 12 mm and thickness of 3.4 mm produce tactile stimulation on human skin. The control signal is generated by PC (Fig. 8).

As it follows from the graph of vibration motors FM34F motor characteristic, the relationship between voltage (current) and frequency is essentially linear. Therefore, the level of current in tactor circuit corresponds the level of vibration. The tactile display was connected to the Motor Driver Unit controlled by the signals from D/A board.

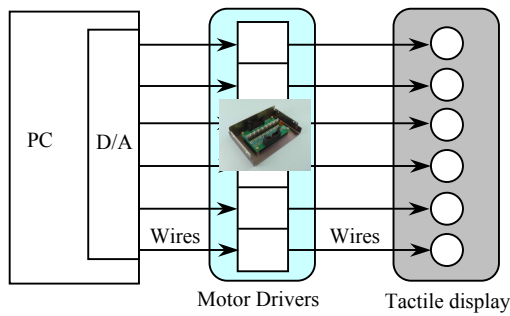


Figure 8. Control system of BraTact

5 USER STUDY METHODOLOGY

5.1 Apparatus

A developed tactile display *BraTact* was used to present the shape, and stiffness of object. The smallest participant's forearm circumference was 21 cm, so the distance between factors always was 3.5 cm or more, i.e. larger than a single receptive field (about 2.5 cm [16]).

5.2 Participants

A total of 5 males and 1 female with no previous knowledge about experiment were examined. Their age varied from 23 to 31.

The participants were recruited among the students and staff of the Tachi Laboratory of the University of Tokyo and did not receive any compensation for their participation. None of the subjects reported any sensory difficulties.

5.3 Procedure and Stimuli

Object shape presentation. Object shape information is important for operator. While colliding, the objects with smooth shape attenuate the impact forces. Thus, knowledge of object shape can improve performance of motion planning in cluttered environment. The intuitive approach of representation of simple object shapes (circle (Pattern A), rectangle (B), triangle (C)) and shape primitives (arc (D), line (E), point (F)) is presented in Fig. 9. The dashed ovals depict the active factors.

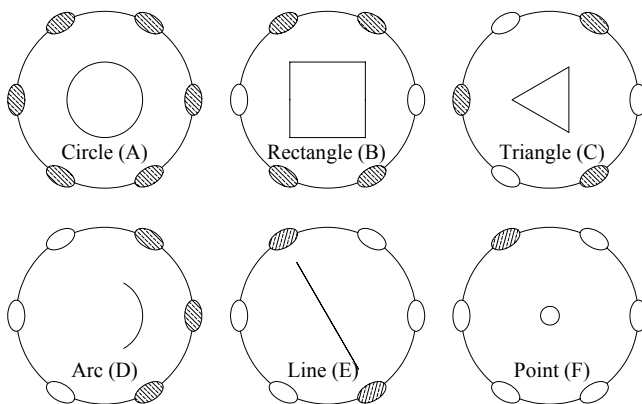


Figure 9. Tactile presentation of the object shape

Dynamic Shapes Experiment was aimed at presenting the shapes in a more transparent manner. The duration time of factor activation for all shapes was the same - 2 sec. For round, rectangular and triangular shape, the factors were activated one by one in counter-clockwise direction. This allows the human to draw in his mind the path represented by factor. The arc was

presented by simultaneous activation of all three factors, but with time-varying intensities with duration of 2 sec. Moreover, intensity level in the middle factor was larger than in neighboring ones. To draw the line, we tried to reproduce the apparent motion illusion. For that, two factors were activated simultaneously but with opposite time-varying intensities levels. That is, when the first factor had the maximum vibration intensity the opposite factor had the lowest intensity and vice versa. The point was presented by activation of single factor with ramp signal.

Stiffness presentation. In *Static Stiffness Experiment* all factors were activated simultaneously with the same intensity level of 2 sec. duration. Five vibration intensity levels (Level 1 (167 Hz) (Pattern A), Level 2 (188 Hz) (B), Level 3 (208 Hz) (C), Level 4 (229 Hz) (D), Level 5 (250 Hz) (E)) representing object stiffness from very low rate to very high were chosen. The darkness level of gray color in Fig. 10 represents the vibration amplitude level.

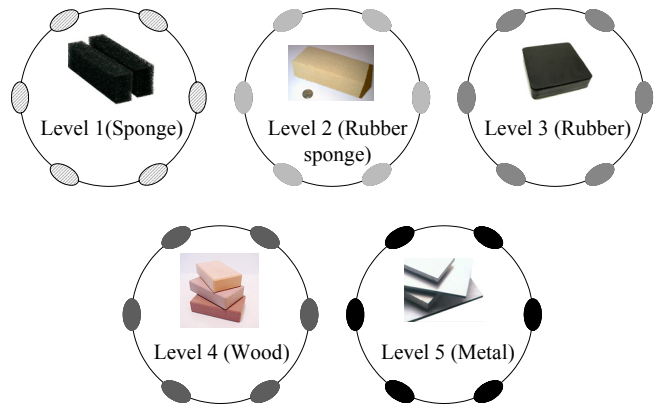


Figure 10. Tactile presentation of the object stiffness

In *Dynamic Stiffness Experiment* all factors were activated simultaneously for given level but with time-varying intensity. The time-dependent pattern was chosen to represent the contact point motion during contact transient (when we collide with stiff object our arm immediately stops moving forward). The stiffest material, aluminum, was presented as short ramp impulse with duration of 0.3 sec. The less stiff material the longer duration and smaller amplitude of impulse were presented to human's forearm skin. To mimic nonlinearity of the sponge material (see Fig. 2(a)), the sine wave pattern was presented with duration of 2 sec.

The experiment procedure is as follows. To mask auditory cues of the factor vibration, subjects wore headphones producing pink noise of 65 dBA. They were asked to sit down at the table and grasp vertical stick at the edge of the table to establish static reference position. The arm with attached display *BraTact* was not limited by physical constraints and was relaxed. These experimental conditions imitate normal position of the operator's arm. The elastic belt embedded in *BraTact* device provided tight contact of motors and skin. Subjects were informed that the experiment aimed at testing their ability to discriminate between various patterns. Additionally, they were shown a diagram of possible patterns of shape and stiffness presentation. All the participants were given 18 trials practice sessions before experiment for object presentation and 15 trials for stiffness presentation (each pattern was presented 3 times). They were allowed to look at the visual representation of the patterns at all times of practice session and to identify them.

In total, 30 stimuli (6 patterns were repeated 5 times in a random order) were presented during object shape discrimination experiment and 25 stimuli (5 patterns were repeated 5 times in a random order) for object stiffness recognition experiment. The total number of stimuli sensed by participants equals 110

(including static and dynamic mode). After each stimulus, the subject marked the table cell corresponding to the pattern had been detected. The subjects were limited to answer within 10 second. The average duration of four sessions of experiment was 40 min.

6 RESULTS AND DISCUSSION

The results of user study are listed in Table 4 - Table 7.

Table 4. Group Mean Percentage of Recognition of Shape in Dynamics

Group Mean Percentage, %	Subject Response						
	Actual Pattern	A	B	C	D	E	F
A	100.0	0	0	0	0	0	0
B	0	83.3	13.3	0	0	0	3.3
C	0	3.3	96.7	0	0	0	0
D	3.3	0	0	73.3	10.0	13.3	0
E	3.3	3.3	3.3	3.3	86.7	0	0
F	0	3.3	0	0	3.3	93.3	0

Table 5. Group Mean Percentage of Recognition of Shape in Static Condition

Group Mean Percentage, %	Subject Response						
	Actual Pattern	A	B	C	D	E	F
A	60.0	26.7	6.7	3.3	3.3	0	0
B	33.3	26.7	26.7	3.3	10.0	0	0
C	10.0	33.3	43.3	0	13.3	0	0
D	0	3.3	6.7	76.7	10.0	3.3	0
E	0	10.0	20.0	16.7	53.3	0	0
F	0	0	0	0	3.3	96.7	0

Table 6. Group Mean Percentage of Recognition of Stiffness in Dynamics

Group Mean Percentage, %	Subject Response					
	Actual Pattern	A	B	C	D	E
A	100.0	0	0	0	0	0
B	0	80.0	13.3	6.7	0	0
C	0	16.7	73.3	10.0	0	0
D	0	0	20.0	70.0	10.0	0
E	0	0	0	3.3	96.7	0

Table 7. Group Mean Percentage of Recognition of Stiffness in Static Condition

Group Mean Percentage, %	Subject Response					
	Actual Pattern	A	B	C	D	E
A	73.3	20.0	6.7	0	0	0
B	13.3	50.0	16.7	20.0	0	0
C	0	16.7	50.0	20.0	13.3	0
D	0	0	23.3	53.3	23.3	0
E	0	0	6.7	23.3	70.0	0

The ANOVA results revealed that it was significantly easier for participants to recognize stiffness of materials B ($p=0.001<0.05$) and E ($p=0.04<0.05$) during Dynamic Condition than in Static Condition. Shape patterns A, B, and C were significantly easier to recognize during Dynamic Condition than in Static Condition ($p=0.006<0.05$, $p=0.002<0.05$, and $p=0.007<0.05$, correspondingly). The important point is that the recognition rate of the line presented by apparent motion illusion was much more higher than that of line presented in *Static* mode. Based on this evidence, we can use this effect to draw more complex shapes.

7 CONCLUSION

The increasing complexity of tasks performed by teleoperation systems requires to deliver and to display tactile information to the human operator effectively in order to ensure safe and efficient interaction with environment. The sensory system of the developed slave robot supports the local admittance controllers generating compliant motion with information on exerted force. The methods of object stiffness estimation and object shape recognition were elaborated. These approaches can also be extended for object exploration in 3D space.

The tactile display *BraTact* supporting the presentation of tactile information by means of the bracelet with tactors was developed. The results of the user study revealed that the Dynamic mode of presentation of the object properties was more intuitive, and, therefore, resulted in very high level of discrimination accuracy. The future step is elaboration of the concept of “*Dynamic tactile drawing*”, when graphical information is presented by tactile patterns generated discretely in time.

Acknowledgments. The research is supported in part by a Japan Society for the Promotion of Science (JSPS).

REFERENCES

- [1] E. R. Kandel, J. H. Schwartz, and T. M. Jessell. *Principles of Neural Science*. New York: McGraw-Hill, 2000.
- [2] Optic fiber tactile sensor Kinotex, Nitta Corporation. [Online]. Available: <http://www.nitta.co.jp/>
- [3] J. Serra. *Image Analysis and Mathematical Morphology*. London: Academic Press, 1982.
- [4] R.L. Klatzky and S. Lederman. Intelligent exploration by the human hand. *Dexterous Robot Manipulation*. S.T. Venkataraman and T. Iberall, Ed. New York: Springer-Verlag, pages 66–81, 1990.
- [5] F. Yamaguchi. *Curves and Surfaces in Computer Aided Geometric Design*. Berlin: Springer-Verlag, 1988.
- [6] PHANTOM line of haptic devices. [Online]. Available: <http://www.sensable.com>
- [7] CyberGrasp. [Online]. Available: <http://www.immersion.com>
- [8] J.B.F. van Erp and H.A.H.C. van Veen. A multi-purpose tactile vest for astronauts in the international space station. In *Proc. Int. Conf. EuroHaptics*, pages 405–408, Dublin, 2003.
- [9] R. D. Howe, D. A. Kontarinis, and W. J. Peine. Shape memory alloy actuator controller design for tactile displays. In *Proc. 34th IEEE Conf. on Decision and Control*, pages 3540–3544, 1995.
- [10] H.A.H.C. van Veen and J.B.F. van Erp. Providing directional information with tactile torso displays. In *Proc. Int. Conf. EuroHaptics*, pp. 471–474, Dublin, 2003.
- [11] R.W. Cholewiak. The perception of tactile distance: Influences of body site, space, and time. *Perception*, 28(7):851–875, 1999.
- [12] R. W. Lindeman, Y. Yanagida, H. Noma, and K. Hosaka. Wearable vibrotactile system for virtual contact and information display. *Virtual Reality*, 9:203–213, 2006.
- [13] I. Oakley, Y. Kim, J. Lee, and J. Ryu. Determining the feasibility of forearm mounted vibrotactile displays. In *Proc. Symp. on Haptic Interfaces and Teleoperator System*, pages 27–34, Alexandria, VA, 2006.
- [14] E. Piatetski and L. Jones. Vibrotactile pattern recognition on the arm and torso. In *Proc. First Joint EuroHaptics Conf. and Symp. on Haptic Interfaces for Virtual Environment and Teleoperator System*, pages 18–24, Pisa, 2005.
- [15] H-Y. Chen, J. Santos, M. Graves, K. Kim, and H. Z. Tan. Tactor localization at the wrist. In *Proc. Int. Conf. EuroHaptics*, pages 209–218, Madrid, 2008.
- [16] R.W. Cholewiak and A.A. Collins. Vibrotactile localization on the arm: Effects of place, space, and age. *Perception and Psychophysics*, 65:1058-1077, 2003.